Electronic Supplementary Material (ESI) for Journal of Materials Chemistry B.

Perylene Diimide Zwitterionic Polymer for Photoacoustic Imaging Guided Photothermal/Photodynamic Synergetic Therapy with Single Near-Infrared

Pengfei Sun, [a†] Xiaoxiao Wang, [a†] Gaina Wang, [a] Weixing Deng, [a] Qingming Shen, [a] Rongcui Jiang, [a] Wenjun Wang, [b] Quli Fan, [*, a] and Wei Huang, [c]

[a] Key Laboratory for Organic Electronics and Information Displays & Jiangsu Key Laboratory for Biosensors, Institute of Advanced Materials (IAM), Jiangsu National Synergetic Innovation Center for Advanced Materials (SICAM), Nanjing University of Posts & Telecommunications, 9 Wenyuan Road, Nanjing 210023, China.

[b] Key Lab of Optical Communication Science and Technology of Shandong Province & School of Physics Science and Information Engineering, Liaocheng University, Liaocheng 252059, China.

[c] Shaanxi Institute of Flexible Electronics (SIFE), Northwestern Polytechnical University (NPU), 127 West Youyi Road, Xi'an 710072, Shaanxi, China.

[†] These authors contributed equally to this work.

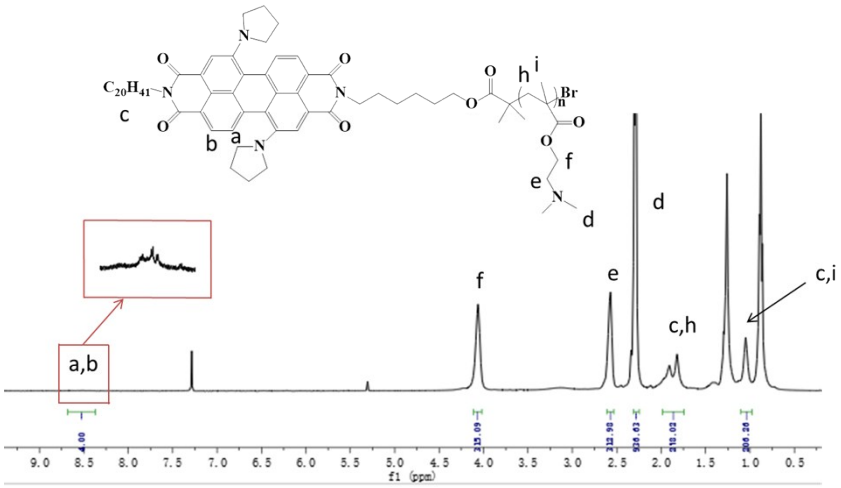

Figure S1. ^{1}H-NMR spectra of PDMAEMA-PDI in $CDCl_3$.

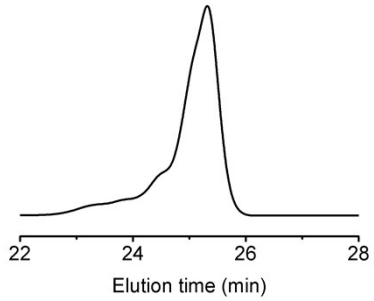

Figure S2. The GPC curve of PDMAEMA-PDI.

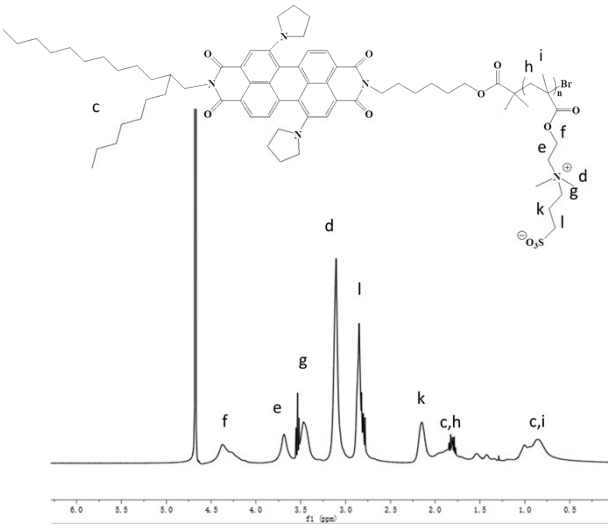

Figure S3. ^{1}H-NMR spectra of PDS-PDI in D_2O.

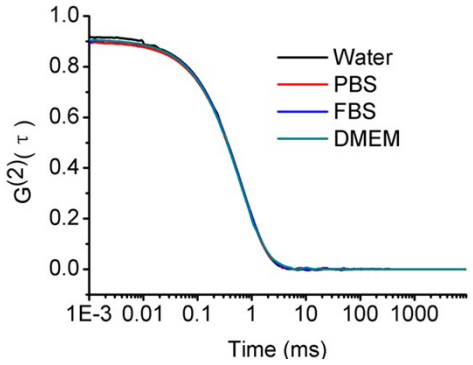

Figure S4. Auto correlation function obtained by DLS analysis (θ = 90º) of PDS-PDI in different solvent (Water, PBS, FBS, DMEM).

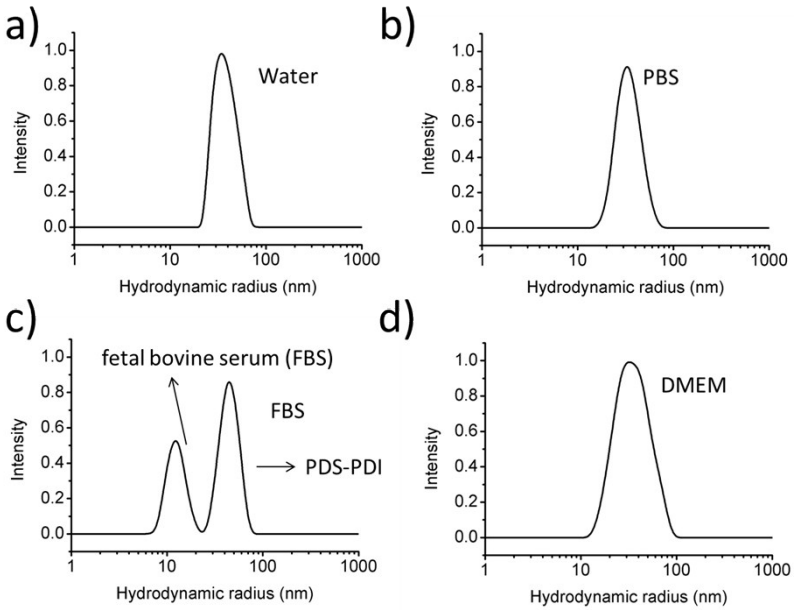

Figure S5. The hydrodynamic radius ($\langle R_h \rangle$) of PDS-PDI in different solvent. a) Water, b) PBS, c) FBS, d) DMEM.

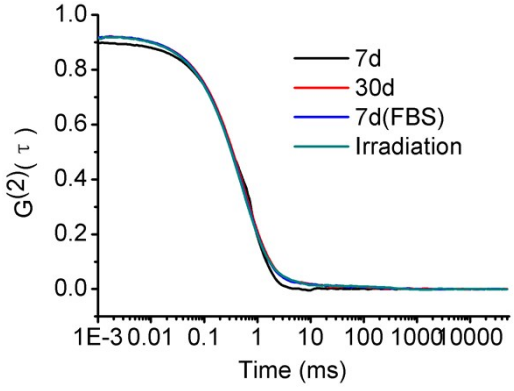

Figure S6. Auto correlation function obtained by DLS analysis (θ = 90º) of PDS-PDI by different treatment (after 7 d, 30 d in water, after 7 d in FBS, after irradiation for 30 min (660 nm, 1.0 W cm^{-2})).

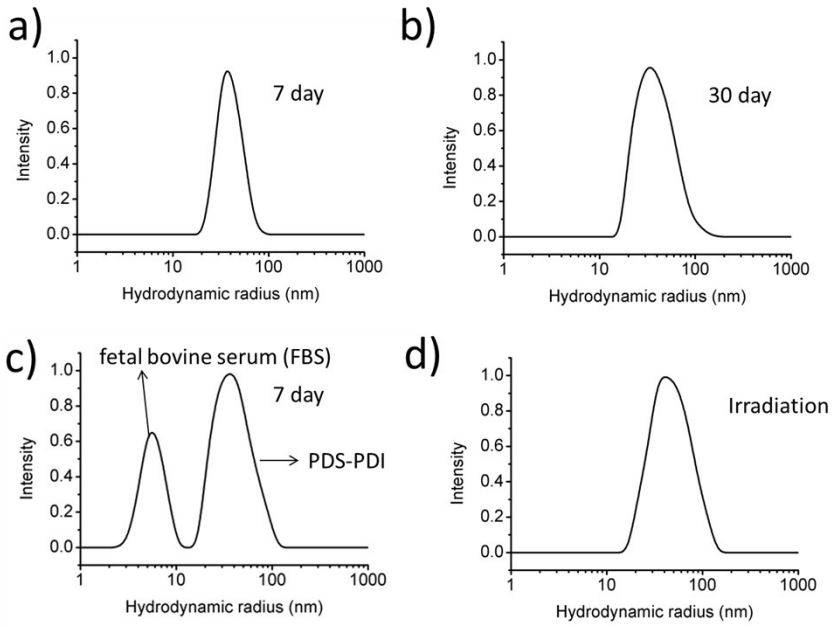

Figure S7. a) 7 days, b) 30 days, the hydrodynamic radius ($\langle R_h \rangle$) of PDS-PDI in water. c) $\langle R_h \rangle$ of PDS-PDI in FBS after 7 days. d) $\langle R_h \rangle$ of PDS-PDI aqueous solution after irradiation for 30 min (660nm, 1.0 W cm^{-2}).

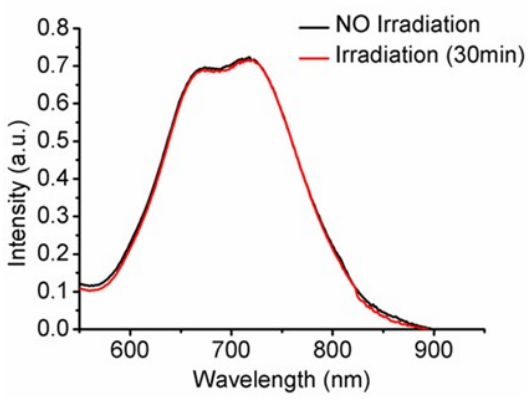

Figure S8. UV-vis-NIR spectra of PDS-PDI in water with laser irradiation for 30 min (660 nm laser with a power intensity of 1.0 W cm^{-2}).

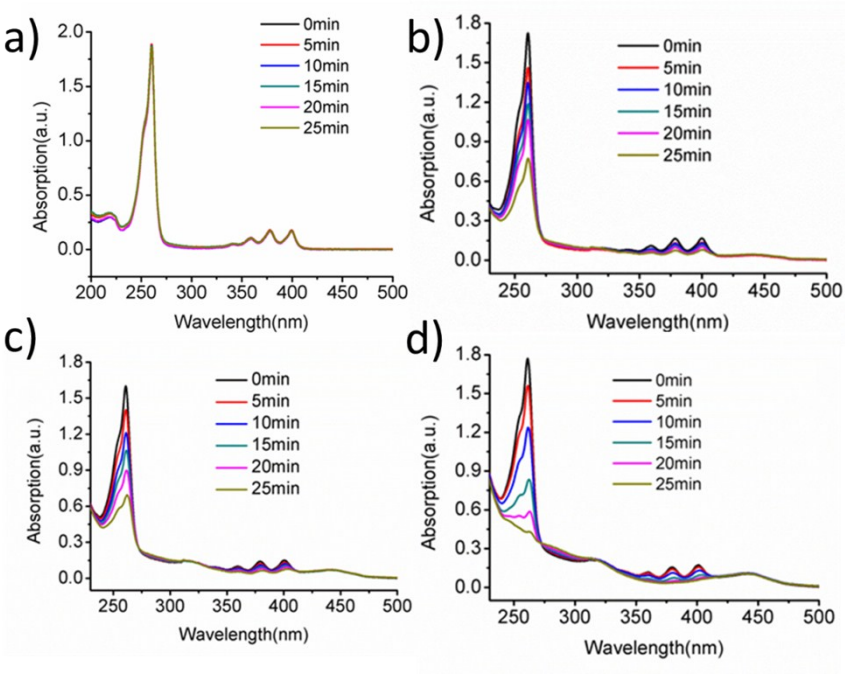

Figure S9. a) Absorbance of ADMA after photodecomposition by ROS generation upon laser irradiation without PDS-PDI. b) 0.0625 mg mL^{-1}, c) 0.125 mg mL^{-1}, d) 0.5 mg mL^{-1}, absorbance of ADMA after photodecomposition by ROS generation upon laser irradiation with PDS-PDI.

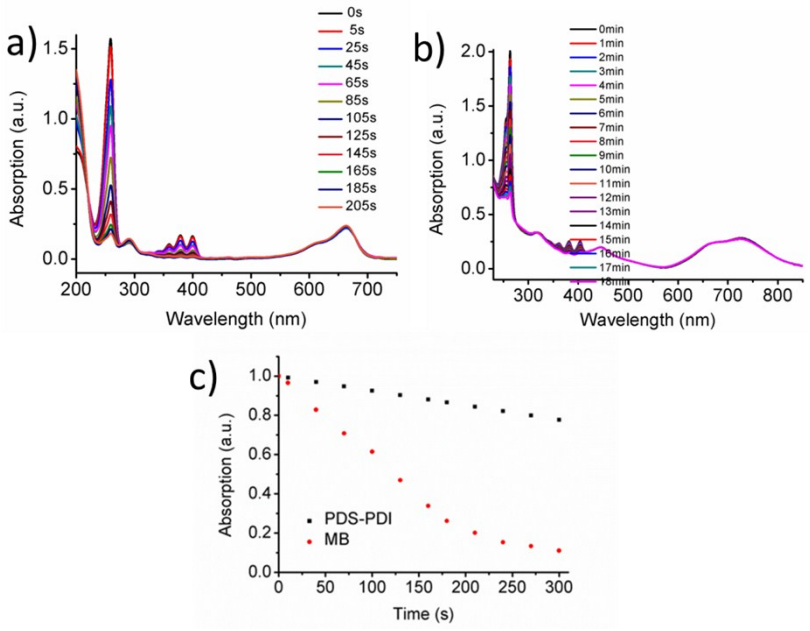

Figure S10. The singlet oxygen production efficiency of PDS-PDI aqueous solution. a) Absorbance of ADMA after photodecomposition by ROS generation upon laser

irradiation with MB (660 nm, 0.5 W cm^{-2}). b) With PDS-PDI (660 nm, 0.5 W cm^{-2}). c) Time-dependent absorption of ADMA at 264 nm under laser irradiation.

Singlet oxygen quantum yields were calculated according to the equation:

$$\Phi_{\Delta}(PS) = \Phi_{\Delta}(MB) \times \frac{\mathrm{m}(PS)}{\mathrm{m}(MB)} \times \frac{F(MB)}{F(PS)} \quad (1)$$

where PS and MB designate photosensitizer and methylene blue respectively. $\phi_{\Delta}(MB)$ is the singlet oxygen quantum yield of MB free in water given as 0.52. m is the slope of difference in change in absorbance of ADMA at absorbance maxima with the irradiation time. F is the absorption correction factor, which is given as $F = 1 - 10^{-OD}$.

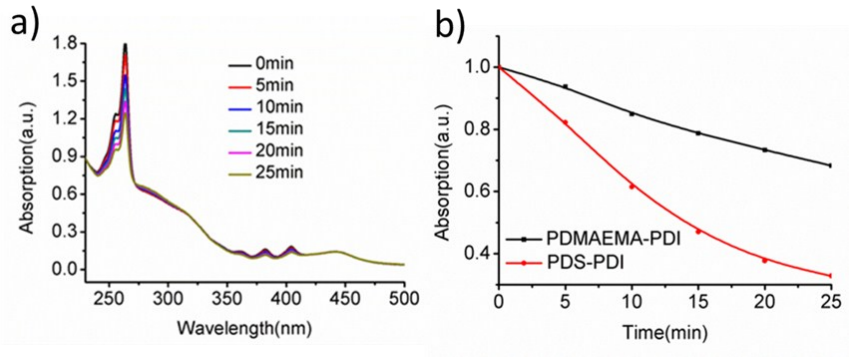

Figure S11. a) Absorbance of ADMA after photodecomposition by ROS generation upon laser irradiation with PDMAEMA-PDI. b) Time-dependent absorption of ADMA at 264 nm under laser irradiation (The same concentration of PDMAEMA-PDI and PDS-PDI).

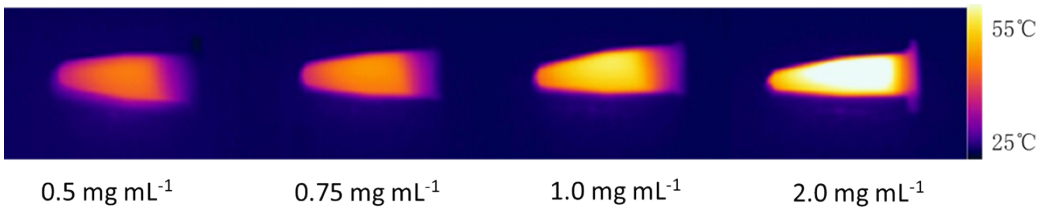

Figure S12. The thermal images of polymer PDS-PDI aqueous solution with different concentrations.

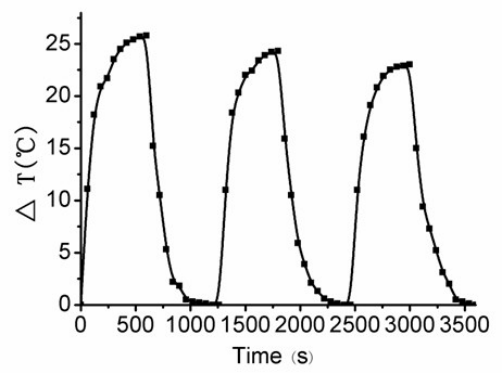

Figure S13. The thermal cycling of polymer PDS-PDI aqueous solution (660 nm, 0.5 W cm^{-2}).

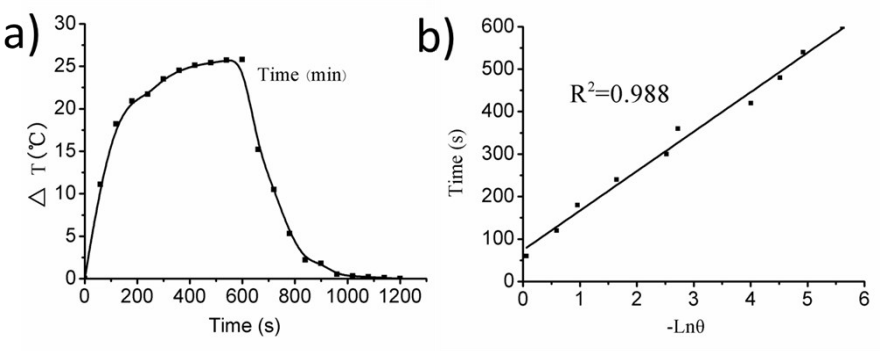

Figure S14. The photothermal conversion efficiency of polymer PDS-PDI aqueous solution. a) The photothermal response of the aqueous solution of PDS-PDI (0.5 mg mL^{-1}) for 600 s with a NIR laser (660 nm, 0.5 W cm^{-2}) and then the laser was shut off. b) Linear time data versus -Ln θ obtained from the cooling period of Figure S13a.

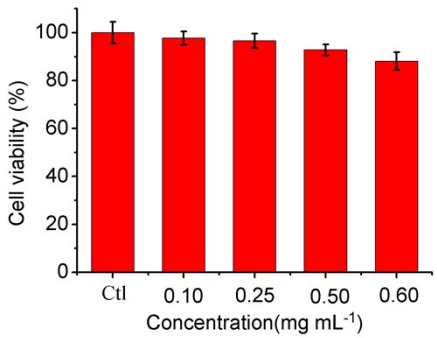

Figure S15. Cell viabilities of MDA-MB-231 cells incubated for 24 h with at different concentrations polymer PDS-PDI (0-0.6 mg mL^{-1}) without laser irradiation.

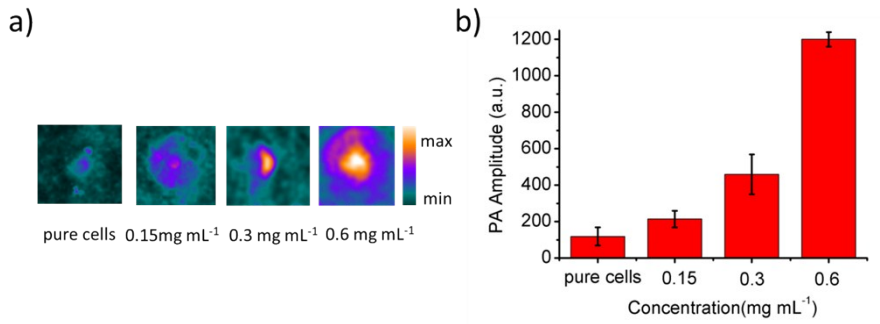

Figure S16. (a) The PA imaging and (b) PA intensity of pure MDA-MB-231 cells and MDA-MB-231 cells after 4 h incubated with different concentrations PDS-PDI.

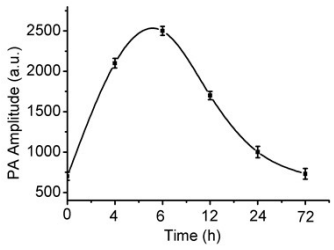

Figure S17. Real-time monitoring of the PA intensity changes of blood post injection of PDS-PDI (2 mg mL^{-1},100 uL).

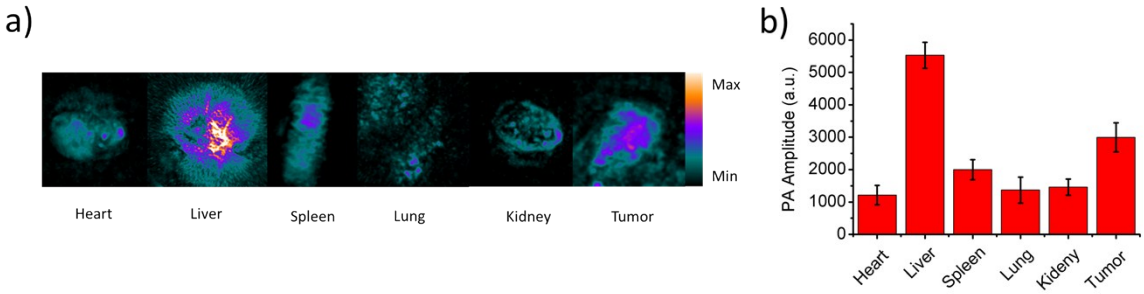

Figure S18. Biodistribution analysis of PDS-PDI by PA imaging. a) *Ex vivo* PA imaging of main organs after 24 h injection of PDS-PDI. b) Quantification of PA signal intensity of main organs after 24 h injection of PDS-PDI.

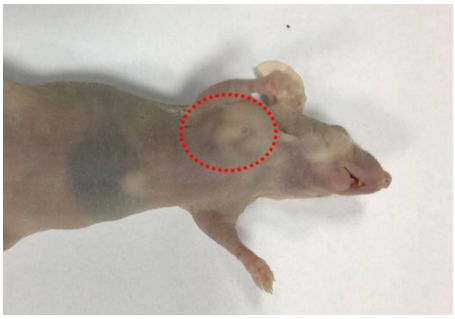

Figure S19. A bright field image of MDA-MB-231 tumor-bearing mice for *in vivo* photothermal test.

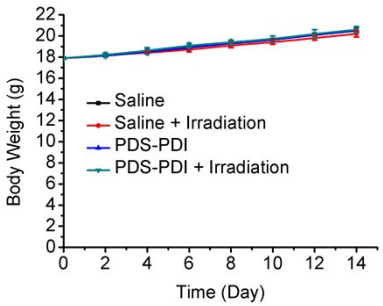

Figure S20. Body weight curves of MDA-MB-231 tumor-bearing mice for four treatment groups.

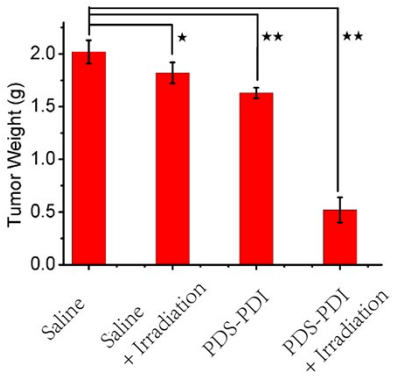

Figure S21. MDA-MB-231tumor weight, sacrificed mice from the four treatment groups.

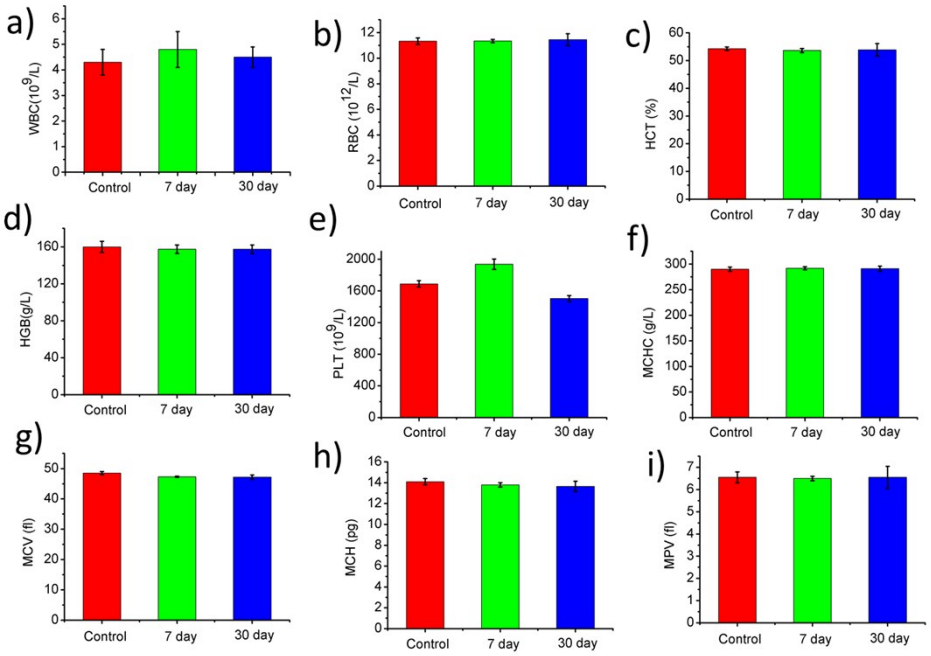

Figure S22. Blood routines of mice examination were measured after the treatment with polymer PDS-PDI (2 mg mL^{-1}, 100 uL) during 30 day.